Geophysical Journal International

Geophys. J. Int. (2013) doi: 10.1093/gji/ggt298

Geophysical Journal International Advance Access published August 28, 2013

Testing the accelerating moment release (AMR) hypothesis in areas of high stress

Aurélie Guilhem,[1,*] Roland Bürgmann,[1] Andrew M. Freed[2] and Syed Tabrez Ali[2,†]

[1] *Berkeley Seismological Laboratory, University of California, Berkeley,* 215 *McCone Hall, Berkeley, CA* 94720-4670*, USA.*
E-mail: aurelie@seismo.berkeley.edu
[2] *Department of Earth & Atmospheric Sciences, Purdue University,* 550 *Stadium Mall Drive, West Lafayette, IN* 47907-2051*, USA*

Accepted 2013 July 22. Received 2013 July 17; in original form 2013 January 28

SUMMARY

Several retrospective analyses have proposed that significant increases in moment release occurred prior to many large earthquakes of recent times. However, the finding of accelerating moment release (AMR) strongly depends on the choice of three parameters: (1) magnitude range, (2) area being considered surrounding the events and (3) the time period prior to the large earthquakes. Consequently, the AMR analysis has been criticized as being *a posteriori* data-fitting exercise with no new predictive power. As AMR has been hypothesized to relate to changes in the state of stress around the eventual epicentre, we compare here AMR results to models of stress accumulation in California. Instead of assuming a complete stress drop on all surrounding fault segments implied by a back-slip stress lobe method, we consider that stress evolves dynamically, punctuated by the occurrence of earthquakes, and governed by the elastic and viscous properties of the lithosphere. We study the seismicity of southern California and extract events for AMR calculations following the systematic approach employed in previous studies. We present several sensitivity tests of the method, as well as grid-search analyses over the region between 1955 and 2005 using fixed magnitude range, radius of the search area and period of time. The results are compared to the occurrence of large events and to maps of Coulomb stress changes. The Coulomb stress maps are compiled using the coseismic stress from all $M > 7.0$ earthquakes since 1812, their subsequent post-seismic relaxation, and the interseismic strain accumulation. We find no convincing correlation of seismicity rate changes in recent decades with areas of high stress that would support the AMR hypothesis. Furthermore, this indicates limited utility for practical earthquake hazard analysis in southern California, and possibly other regions.

Key words: Earthquake interaction, forecasting, and prediction; Seismicity and tectonics; Fractures and faults; Crustal structure.

1 INTRODUCTION

The search for evidence of spatiotemporal interactions between earthquakes is fundamental for understanding the evolution of stress in the lithosphere and the associated distribution of earthquakes in space and time. The elastic rebound theory by Reid (1910) first introduced the relationship between elastic stress accumulated along a fault zone and earthquake occurrence. The recognition that continuous plate motions are primarily accommodated by earthquakes on major faults, releasing the accumulated stress since the last main shock, constitutes the basic premise of earthquake forecasting. This is especially true if one can quantify the slip-deficit accumulation rate, the time since the last earthquakes (or the times between several events) and the slip of a characteristic event. If it were possible to establish from seismicity patterns that stress has reached near-critical levels, it might be possible to improve upon such 'standard' forecasting approaches.

Over the past decades, several retrospective analyses for precursory seismicity patterns, which consider the evolution of seismicity in relation to rising stress levels, have been undertaken. These studies have focused on both simple changes in the rate of seismicity (i.e. quiescence and activation) as well as on more complex spatial and temporal patterns. It has been suggested that significant increases in moment release occurred in years to decades prior to many large

*Now at: Swiss Seismological Service, ETH Zürich H NO66, Sonneggstrasse 5, 8092 Zürich, Switzerland.
†Now at: Department of Geoscience, University of Wisconsin-Madison, 1215 W. Dayton St., Madison, WI 53706, USA.

earthquakes of recent times (Ellsworth *et al.* 1981; Kanamori 1981; Lindh 1990; Sykes & Jaumé 1990; Bufe & Varnes 1993; Bowman *et al.* 1998; Bowman & King 2001; Sammis *et al.* 2004). The accelerating moment release (AMR) hypothesis promoted by Bowman *et al.* (1998) is based on a simple physical model linking static stress changes in the lithosphere to increases in the rate of smaller sized earthquakes before a main shock. The underlying hypothesis formulated by Bowman & King (2001) and later by King & Bowman (2003) is that AMR informs on the decay of the stress shadow from a large past earthquake prior to the next one, considering the stress loading in the interseismic period. According to this model, immediately after an earthquake, static stress changes unload the crust in the vicinity of the fault that ruptured, and earthquake occurrence is expected to be low where stress levels fall below the failure threshold. As time progresses in the earthquake cycle, the stress shadow retracts because of tectonic loading, and earthquakes occur as the local stress conditions evolve. AMR was retrospectively demonstrated for all eight M6.5+ earthquakes between 1950 and 1994 in southern California (Bowman *et al.* 1998). If correct, this hypothesis has significant potential for earthquake forecasting as suggested by Jiang & Wu (2005) who performed a systematic search for AMR in China between 1970 and 2003 and reported accelerating seismicity prior to the majority of the 65 studied earthquakes. Mignan (2011) provided a comprehensive review of publications on accelerating seismicity preceding major earthquakes.

However, evidence for AMR in retrospective studies strongly depends on the choice of several parameters, such as the magnitude range of earthquakes included in the analysis, the area surrounding the main shock being considered and the length of the time period prior to a target event (Jiang & Wu 2006; Hardebeck *et al.* 2008). Some AMR studies found that these three variables have to be appropriately scaled with the magnitude of the main shock (Bowman *et al.* 1998; Wang *et al.* 2004; Jiang & Wu 2005). Initial AMR studies used a search over circular regions of various radii (Bowman *et al.* 1998; Jiang & Wu 2005), while a more recent approach has been to consider the critical region of high stress determined with a back-slip dislocation model of the studied main shock rupture (Bowman & King 2001; King & Bowman 2003; Mignan *et al.* 2006a,b). Both methods (i.e. circular region and back-slip model) have raised doubts about their utility (Michael *et al.* 2006; Hardebeck *et al.* 2008). First of all, criticisms have focused on the choice of the three variables in the AMR analysis, which appear to be case-specific (i.e. they are generally optimized to produce AMR for a given historic event). In addition, the use of the back-slip dislocation model for earthquake forecasting is problematic, since it requires *a priori* knowledge of the fault segments that will rupture. The published observations of apparent AMR have been suggested to be the result of a 'data-fitting exercise', in which the search variables were tuned such as to maximize the apparent AMR behaviour prior to historic main shocks (Michael *et al.* 2006; Hardebeck *et al.* 2008). Hardebeck *et al.* (2008) concluded that apparent observations of AMR in California and Nevada resulted from a combination of data-fitting and the inherent spatiotemporal clustering of earthquakes.

Despite a number of critical evaluations of AMR (Hardebeck *et al.* 2008; Hough 2009), it continues to be an active area of research. For example, Mignan (2012) showed in the case of the 2009 L'Aquila, Italy, earthquake that a precursory signal (including AMR) became significant only when microseismicity ($M < 3.4$) was included, hence questioning the results of Hardebeck *et al.* (2008) who used $M \geq 4$ events. Mignan (2011, 2012) also argued that AMR might not systematically appear before all large earthquakes, and may be affected by the presence of regional stress heterogeneities larger than the fault-loading field. In addition, Mignan (2008) argued, using seismicity simulations based on the concept of elastic rebound, that the fitting approach (i.e. the c-value) of Bowman *et al.* (1998) provides weak constraints on the space–time window in which synthetic AMR signals are defined. Several recent studies put forward alternative methodologies (Mignan 2008, 2011, 2012; Bouchon *et al.* 2013).

As opposed to previous studies that searched retrospectively for AMR prior to large earthquakes with optimal parameters, we carry out for the first time a systematic grid search for AMR in space and time, and we compare its results with independently developed models of ∼200 yr of stress accumulation in southern California (Freed *et al.* 2007). If seismicity rates do indeed rise in areas where stress increases, and prior to large events, our approach would be the appropriate method to test and implement the AMR concept in earthquake forecasting efforts. To evaluate more directly the underlying concept of enhanced seismicity in areas of high stress and impending large earthquake ruptures, we consider here that lithospheric stress (1) evolves dynamically such that stress accumulates because of the tectonic plate motions, (2) is punctuated by the occurrence of earthquakes and (3) is governed by the elastic and viscous properties of the lithosphere (Freed *et al.* 2007). Thus, we regard a mechanical model of stress evolution over the last two centuries, rather than assuming a complete stress drop on all fault segments surrounding an eventual rupture implied by the back-slip stress lobe method (Bowman & King 2001). As mentioned by Bowman & King (2001), the precise definition of regions with increased stress requires modelling the contributions of events over a long period of time. We rigorously evaluate inferred stress levels determined from physical models of southern California stress evolution that incorporate coseismic stress changes from $M > 6.5$ events since 1812, their corresponding post-seismic relaxation in the viscoelastic lower crust and upper mantle, and the interseismic stress accumulation derived from the current surface strain field (Freed *et al.* 2007). Even if a time period of 200 yr is short with respect to the repeat time intervals of many faults in southern California, we believe that a careful analysis of AMR behaviour in regions of high stress determined from our calculation is justified as a means towards testing the underlying concepts of statistical physics and mechanical fault interaction. Finally, we evaluate the performance of the AMR approach by focusing on the region of the quasi-regular M6 Parkfield, central California main shocks. We evaluate seismicity spanning the last earthquake cycle of this well-studied rupture sequence, and we consider seismic events with magnitudes as low as 2 preceding the 2004 M6 main shock.

2 DATA AND METHOD

2.1 Study area

California is one of the best-studied seismically active regions in the world with both dense seismic and geodetic networks. We study the regional seismicity compiled from the Advanced National Seismic System (ANSS) catalogue between 32°N and 37.5°N latitude, for the time period from 1910 to 2010 (Fig. 1). Because the earthquake catalogue of this region is large, both in terms of duration and magnitude range of the events, it allows for relatively complete AMR analysis. This is especially true after 1950, as pre-1950 seismicity can reflect major instrumentation and data processing changes (Toppozada & Branum 2002; Hardebeck *et al.* 2008). Five

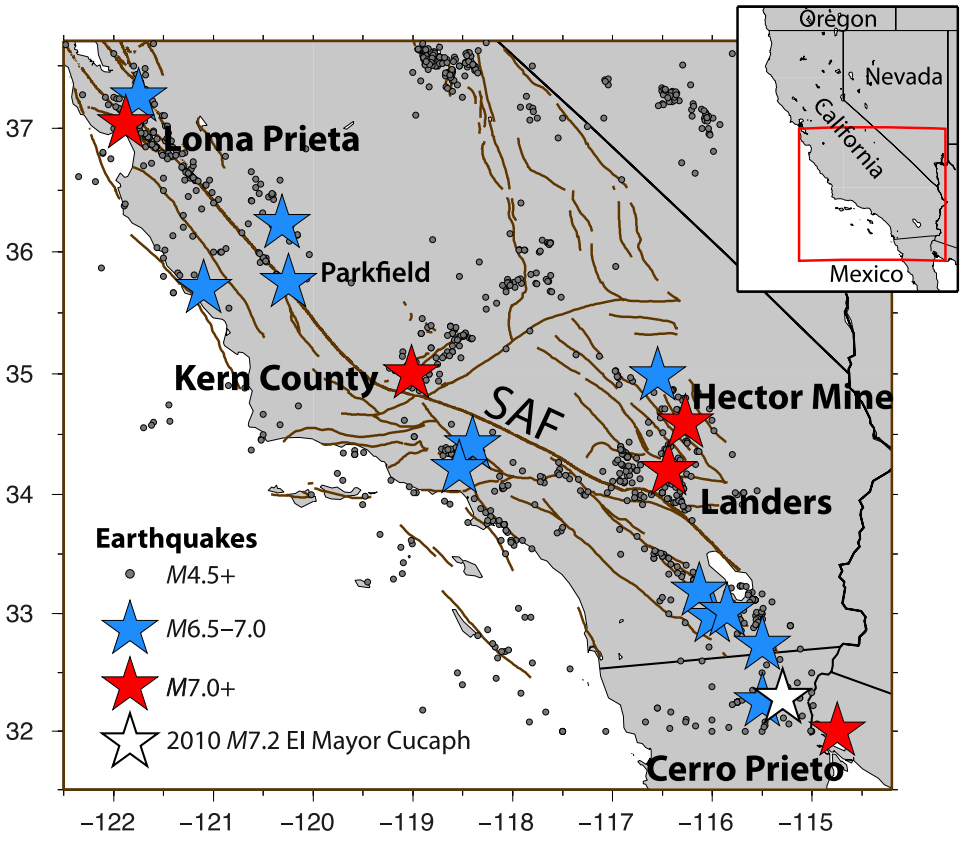

Figure 1. Seismicity map of the study area. The 1910–2010 earthquakes with $M \geq 4.5$ from the ANSS catalogue are the small circles. The $6.5 < M < 7$ events and $M7+$ main shocks are shown by blue and red stars, respectively. The locations of the Parkfield segment and the $M7+$ earthquakes are labelled. The white star shows the 2010 $M7.2$ El Mayor–Cucapah earthquake.

earthquakes with magnitude larger than 7 have been recorded in this time period, the largest one being the $M7.5$ Kern County earthquake in 1952. 12 earthquakes are reported in the catalogue with a magnitude between 6.5 and 7 (Fig. 1).

We later focus on the seismicity in the vicinity of the Parkfield segment along the San Andreas Fault (SAF) in central California, which is the site of moderate-size earthquakes of magnitude 6 that have repeated at fairly regular intervals: 1857, 1881, 1901, 1922, 1934, 1966 and 2004. If seismicity rates vary according to regional stress levels following the stress accumulation model of King & Bowman (2003), AMR should be observed during the entire earthquake cycle and not only in the last several years before a main shock (Mignan *et al.* 2007). The long time between large events, often on the order of a century or more, rarely allows for complete observations of seismicity through an entire earthquake cycle. Thus, the short repeat time in the Parkfield region provides the opportunity to explore changes in regional seismicity rates over earthquake cycles.

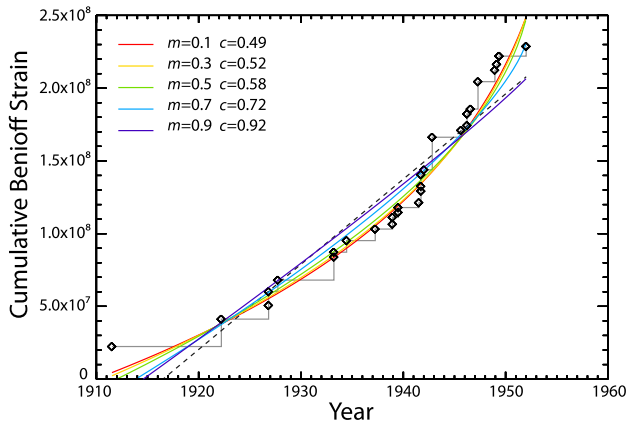

Figure 2. AMR search for the 1952 $M7.5$ Kern County earthquake. The cumulative Benioff strain is shown by the grey line, the linear fit is the dashed line and the colour curves show the power law fitting the data for various values of m (warm colour for low values of m). This AMR calculation uses $5.5 < M < 7.5$ events between 1910 and 1952, within a circular area of 360-km radius around the epicentre (35N, −119E) following the results of Bowman *et al.* (1998). The c-values for each m exponent are given.

2.2 Description of the AMR hypothesis

In the AMR hypothesis, changes in seismicity rate are inferred from an increase over time in the slope of the cumulative Benioff strain prior to a main shock (Bowman *et al.* 1998; King & Bowman 2003; Mignan *et al.* 2007). Fig. 2 shows an example for the $M7.2$ Kern County earthquake, where the observed cumulative Benioff strain, $\varepsilon(t)$, which is derived from the energy (E) of each earthquake (see below):

$$\varepsilon(t) = \sum_{i=1}^{N(t)} \sqrt{E_i(t)} \qquad (1)$$

is fit by a power-law time-to-failure relation (Bowman *et al.* 1998)

$$\varepsilon(t) = A + B\,(t_c - t)^m\,. \quad (2)$$

Here, N is the number of earthquakes considered, t_c is the time for which AMR is being evaluated (i.e. the occurrence time of a large earthquake assuming a retrospective analysis), A is the value of the cumulative Benioff strain at the time of the earthquake t_c, B is a negative fitting constant and m, which determines the curvature of the calculated accelerating moment release curve is often found empirically to be equal to about 0.3 (Bufe & Varnes 1993; Ben-Zion & Lyakhovsky 2002; Mignan *et al.* 2006a). Based on Kanamori & Anderson (1975) the energy (E) in Joules of each particular seismic event is defined as a function of their magnitude (M) by

$$\log(E) = 4.8 + 1.5M. \quad (3)$$

To quantify the AMR, one examines the ratio, called the c-value, between the root-mean-square of the best-fitting power-law time-to-failure function and the root-mean-square of a linear fit to the observed cumulative Benioff strain of the events (eq. 1). If the accelerating power law fits the data better than a linear function, c is less than 1. Bowman *et al.* (1998) defined a successful AMR detection when the c-value is less than 0.7, but other studies used threshold values of the c ratio as low as 0.5 (Bowman & King 2001; Mignan *et al.* 2006a). We generally use the term AMR to refer to the evaluation of this c-value (e.g. Bowman *et al.* 1998; King & Bowman 2003; Mignan *et al.* 2006a), being aware that it has been proposed that there are flaws in that particular methodology such as the consideration of cumulative Benioff strain versus the cumulative number of events or seismic moment, the use of a fixed power exponent m, and the choice to not decluster earthquake catalogues prior to the analysis (Mignan 2011).

The choice of the m exponent is subject to discussion. Ben-Zion & Lyakhovsky (2002) provided a summary of published m exponent values (either fixed or best-fitting values) using critical point theory and continuum mechanics. They found that m ranges from 0.2 to 0.6 with mean values of about 0.3, depending on the choice of magnitude cut-off values. The m exponent can also be inverted for to better fit the observed evolution of regional seismicity (Hardebeck *et al.* 2008). Very low values of $m = 0.1$ have been used to study the earthquake activity prior to the 2009 L'Aquilla, Italy earthquake (De Santis *et al.* 2010). However, Mignan (2011) found that such low values of m reflect very short-term seismic activation, rather than a progressive build-up of stress in the years to decades before a large earthquake. Short-term foreshock sequences before a large earthquake may relate to precursory slow slip transients or other short-term transients lasting days to months as suggested for example by Bouchon *et al.* (2013). Here, we use $m = 0.3$ to directly compare our results with previously published works of Bowman *et al.* (1998) and Bowman & King (2001). Fig. 2 shows the effect of m on the curvature of the power-fit law and its fit with the seismicity prior to the Kern County earthquake. While the c-values get smaller for decreasing m for this earthquake, the differences between the curves are minimal below $m = 0.5$. This supports the logic of employing a single ($m = 0.3$) value for the exponent.

In retrospective studies, the search for AMR requires several parameters to be specified for each target main shock. This includes the magnitude range of the earthquakes considered, the size of the search area, and the length of the time period prior to the target earthquake. Different c-values can be obtained depending on the choice made for the three parameters (Bowman *et al.* 1998). In most previous studies, the variables were optimized to obtain the lowest c-value and as a consequence they lead to the most favourable

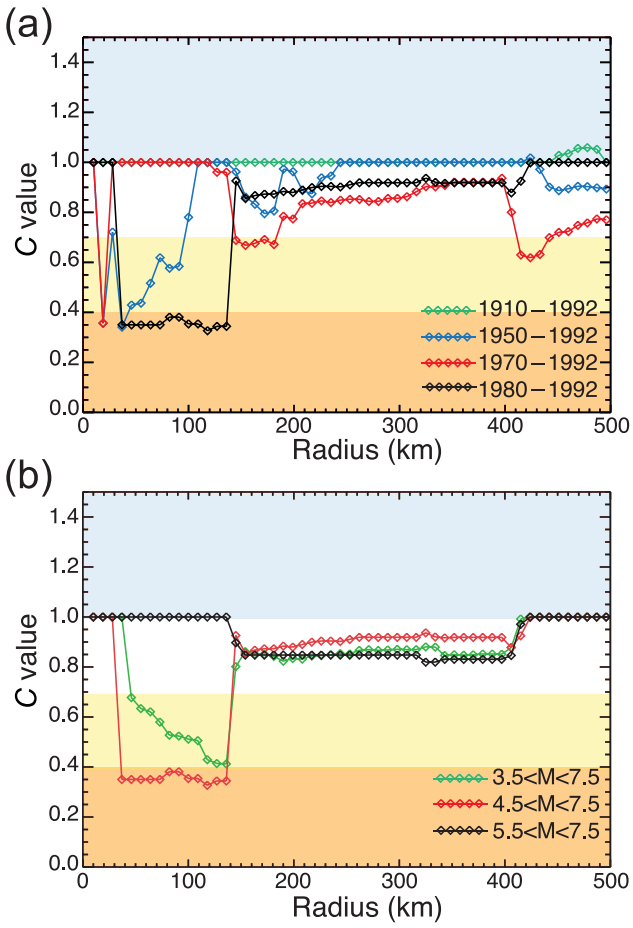

Figure 3. Influence of the time period, magnitude range and circular search area on the analysis of AMR prior to the 1992 M7.4 Landers earthquake. (a) Variation of the considered search period while fixing the magnitude range of catalogue events to $4.5 < M < 7.5$. (b) Variation of the magnitude range with a fixed pre-main shock time period of 12 yr (1980–1992) (Bowman & King 2001). c-Values are fixed to 1 if an insufficient number of events (<7) are included in the spatiotemporal search window.

cases for AMR at the time of known historic main shocks (e.g. see example in Fig. 3). The empirical analyses of AMR found in several regions like in California (Bowman *et al.* 1998), Australia (Wang *et al.* 2004) and Indonesia preceding the great 2004 December Mw9.2 Sumatra earthquake (Jiang & Wu 2005; Mignan *et al.* 2006b) suggest that the optimal region size for best-fitted AMR could possibly scale with the magnitude of the target event, but that the scaling may differ from one region to another (Wang *et al.* 2004; Hardebeck *et al.* 2008). However, there appears to be no clear relation between the duration of the pre-earthquake time period being considered and the magnitude of the main shock. We infer that the cumulative Benioff strain can be better fit by a power-law ($m = 0.3$) time-to-failure function (acceleration of seismicity) when the c-values are less than 0.7, and by a linear trend indicating either no clear change in the seismicity rate and/or deceleration of seismicity when c-values are larger than 1. We require a minimum number of seven earthquakes to follow Bowman's previously published method to calculate the c-value. When this number is not reached either because the chosen distance or time ranges are not large enough or because the minimum magnitude is too large, the c-value is fixed to 1.

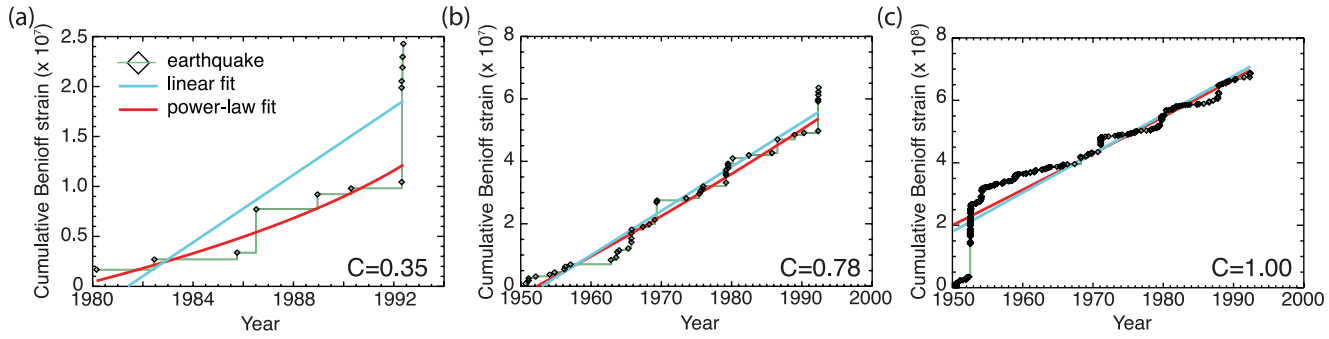

Figure 4. Examples of cumulative Benioff strains obtained for the 1992 Landers earthquake (Fig. 3) exhibiting different behaviours and *c*-values. (a) For 1980–1992, *M*4.5+ earthquakes, and 100 km distance. (b) For 1950–1992, *M*4.5+ earthquakes, and 100 km distance. (c) For 1950–1992, *M*4.5+ earthquakes, and 300 km distance. The Kern County earthquake in 1952 is responsible for the step-like shape of the cumulative Benioff strain in the early time period. In red is the best-fitting power-law trend ($m = 3$) and in blue the best-fitting linear trend of the cumulative Benioff strain.

As shown in Fig. 3, using the example of the 1992 Landers earthquake, the choice of the duration of time considered prior to the main shock (Fig. 3a) and the magnitude range of the seismicity (Fig. 3b) strongly affect the standard AMR analysis for a given search area. Varying the size of the studied region by a small percentage can strongly increase or decrease the number of earthquakes considered as it can include major active fault segments and can result in a strong change of the shape of the cumulative Benioff strain curve (Fig. 4; Hardebeck *et al.* 2008). As demonstrated in Fig. 3 and by Michael *et al.* (2006) and Hardebeck *et al.* (2008), the AMR concept defined by Bowman *et al.* (1998) can be interpreted as a data-fitting exercise. Indeed, there is no general relationship between the search radius, the magnitude range of the catalogue used, and the period of time before the main shock according to its expected magnitude. Most published retrospective AMR studies determine case-specific optimal parameters that produce accelerations in regional seismicity, making it difficult to evaluate any real predictive power of the AMR method (see review by Mignan 2011).

2.3 Grid search application of the AMR method

We perform AMR calculations by extracting events from the ANSS catalogue following the systematic approach employed in previous studies (Bowman *et al.* 1998; Bowman & King 2001). We use Nutcracker, a stress and seismicity analysis software to perform all the AMR calculations and to directly compare our findings with previously published results (Bowman *et al.* 1998; Bowman & King 2001; King & Bowman 2003). We employ the circular search area (Bowman *et al.* 1998) because it is a general method and allows for a systematic grid search for AMR. This is opposed to the more specific approach using the back-slip search that requires knowing in advance the location and size of an anticipated event (Bowman & King 2001).

Rather than optimizing the size of the region, the temporal search window and other parameters in the power-law relation in a retrospective analysis of AMR around historical earthquake ruptures, we carry out a systematic analysis throughout southern California at various times. Jiang & Wu (2006) performed a systematic Benioff strain release analysis in China and presented a set of results using a range of fixed parameters (i.e. 8-yr period, *M*3+ earthquakes and three circular areas whose sizes are dependent on the number of preshocks for each main shock) before 65 *M*6+ earthquakes in China between 1978 and 2003. We follow a similar approach by performing a systematic grid search for AMR across southern California. We use a 30-yr time period, a minimum magnitude for the pre-events of 4.5 to ensure catalogue completeness in particular in remote areas, and three radii for the considered search regions: 150, 200 and 250 km. A 30-yr period represents an average of the time periods fitted for the earthquakes considered by Bowman *et al.* (1998), the shortest one being only 3 yr for the 1983 Coalinga earthquake and the maximum one being 80 yr for the 1989 Loma Prieta main shock. We later compare the information contained in the AMR maps with maps of modelled coseismic, post-seismic and interseismic stress changes over the last century described in the next section (Freed *et al.* 2007). Because both AMR and stress-change maps are meant to give us insights on the relative level of stress within the lithosphere, we search for similarities and differences between the two data sets. For more quantitative comparison, we also compute *c*-values over significantly stressed regions and regions where models suggest low stress in southern California in recent times.

2.4 Stress evolution model

We use the stress evolution model of Freed *et al.* (2007), which considers stress changes over the last 200 yr in the SAF system in southern California, and we search for corresponding seismicity rate increases in areas of high crustal stress. The stress evolution is based on contributions of coseismic, post-seismic and interseismic processes, governed by the elastic and viscous properties of the lithosphere. We calculate Coulomb stress changes based on the critical Coulomb failure criterion at 8 km depth on vertical right-lateral strike-slip faults striking parallel to the SAF (N40°W), assuming an effective coefficient of friction of 0.4 (Freed *et al.* 2007), from all the *M*6.5+ earthquakes since the 1812 Wrightwood earthquake. Finally, we consider the important contributions of post-seismic relaxation processes in time-dependent stress transfer in the last 200 yr (Pollitz & Sacks 1995; Freed *et al.* 2007). Deng & Sykes (1997) showed that a significant percentage of 138 *M*5+ earthquakes from 1932 and 1995 occurred on faults with Coulomb stress increases from major events and interseismic loading since 1812. Similarly, Freed *et al.* (2007) found that about 70 per cent of the events since 1812 occurred in regions that experienced Coulomb stress increase. Both interseismic loading and post-seismic relaxation generally enhanced the area and magnitude of coseismic stress change contributions (Freed *et al.* 2007). Also, they found that the current state of stress is characterized by unrelieved stress increases along the San Bernardino Mountain and Coachella Valley segments of the SAF and the San Jacinto fault zone. Because shallow interseismic fault creep was not incorporated in the models of Freed *et al.* (2007), the creeping central section of the SAF northwest of Parkfield is

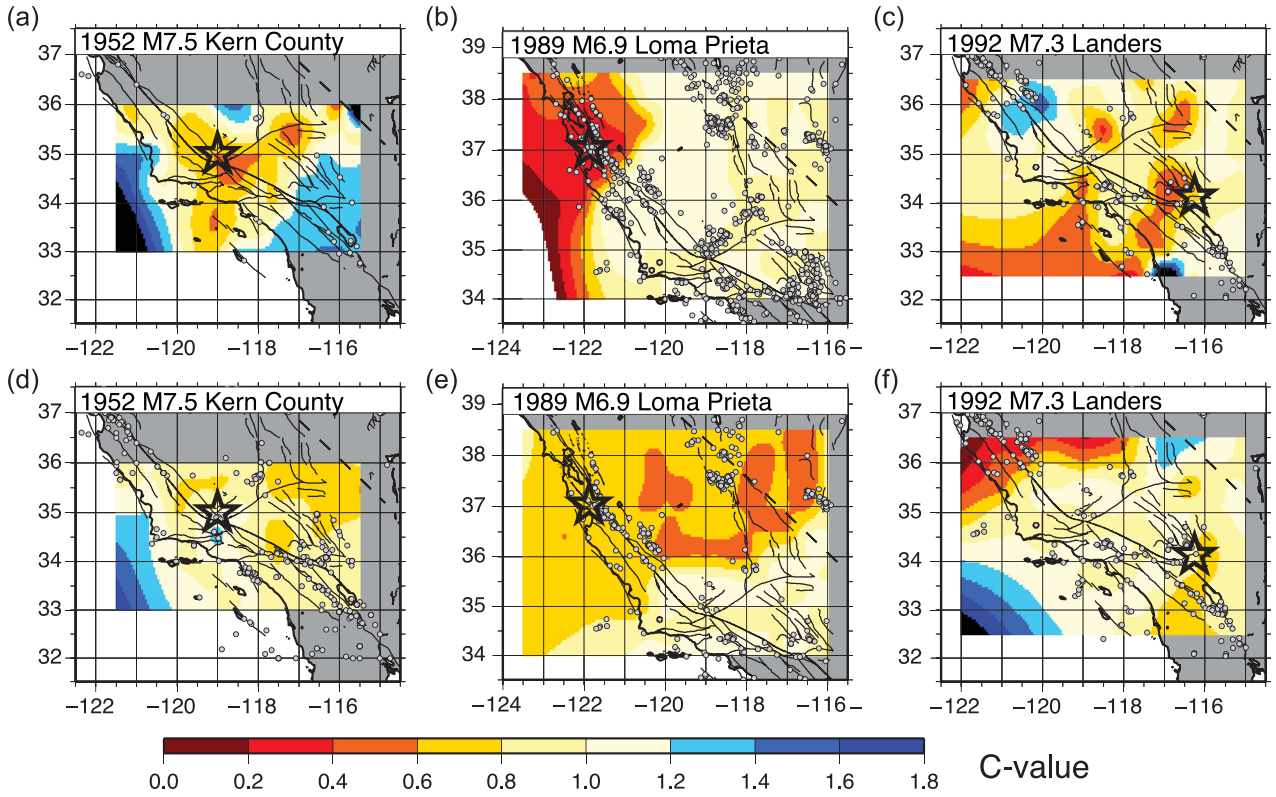

Figure 5. Grid search of AMR with dependent and independent parameters for the *M*7.5 Kern County (a and d), *M*6.9 Loma Prieta (b and e) and *M*7.3 Landers (c and f) earthquakes. (a) Analysis performed with region radius of 325 km and $5.5 < M < 7.5$ events (grey circles) between 1910 and 1952; that is, parameters for Kern County earthquake (star) given by Bowman *et al.* (1998). (b) Analysis performed with region radius of 270 km and $4.5 < M < 7.5$ events (grey circles) between 1910 and 1989, parameters for Loma Prieta (star) given by Bowman *et al.* (1998). (c) Analysis performed with region radius of 125 km and $4.5 < M < 7.5$ events (grey circles) between 1970 and 1992, parameters for Landers (star) given by Bowman *et al.* (1998). (d, e and f) show the results of the analysis using a fixed minimum magnitude of the events (i.e. 4.5), a fixed time period of 30 yr, and a fixed search radius about each gridpoint of 200 km.

modelled as being under apparent high stress. However, creep at rates close to SAF long-term values appears to relax most all strike-slip shear stress in that area (Ryder & Bürgmann 2008). If areas of near-critical stress do indeed experience increasing seismicity rates, AMR should be evident in these areas.

3 RESULTS OF GRID SEARCH FOR AMR

3.1 Grid search with optimal parameters

Considering that AMR is based on the idea that stress and seismicity rates evolve with time around the area of a future earthquake, we apply a grid search for *c*-values at the time of three major earthquakes: *M*7.5 Kern County in 1952, *M*6.9 Loma Prieta in 1989 and *M*7.3 Landers in 1992. Because evidence for strong AMR was published for the three earthquakes (Bowman *et al.* 1998; Bowman & King 2001; King & Bowman 2003), we initially make use of the published fitting parameters and calculate the *c*-values for every point of a grid over the region with an interval of 0.5° in latitude and longitude (Figs 5a–c).

When applying the optimal values for the different variables (i.e. time, magnitude and distance ranges) determined by Bowman & King (2001) for each of the three events, we find that the epicentres are located within the main areas of low *c*-values (Figs 5a–c). The choice made in the AMR parameters in previous studies does not result in other obvious regions of apparent AMR, and low *c*-values are relatively restricted to the epicentral areas. This is encouraging for the AMR hypothesis, showing that the AMR result is relatively stable once the parameters are defined. However as stated previously, we still have to adjust the three parameters for each main shock, and no direct relationship between the region size, time range and the magnitude of the earthquake can be inferred (see also Hardebeck *et al.* 2008; Mignan 2008).

3.2 Grid search with independent parameters

Figs 5(d)–(f) show results for the spatial distribution of the *c*-values for the times of the same three earthquakes assuming the parameter choices described in Section 2.3 (i.e. minimum magnitude of *M*4.5, a distance radius of 200 km and a pre-main shock time period of 30 yr). Contrary to what was obtained when using adjusted parameters, the Kern County and the Loma Prieta earthquake do not locate within an area of significantly low *c*-values. The Landers event on the other hand, is located in a region where *c*-values vary between 0.6 and 0.7 but it does not correspond to the zone where the lowest *c*-values are found.

More generally, Fig. 6 presents a series of maps showing the result of the grid search analysis for a potential major earthquake in southern California in 30-yr intervals using *M*4.5+ earthquakes between 1965 and 2006. The choice of the search radius (i.e. between 100 and 250 km) does not substantially affect the regional pattern of AMR *c*-values in southern California for a given time period. The areas where the *c*-values are either small (i.e. below 0.7) or

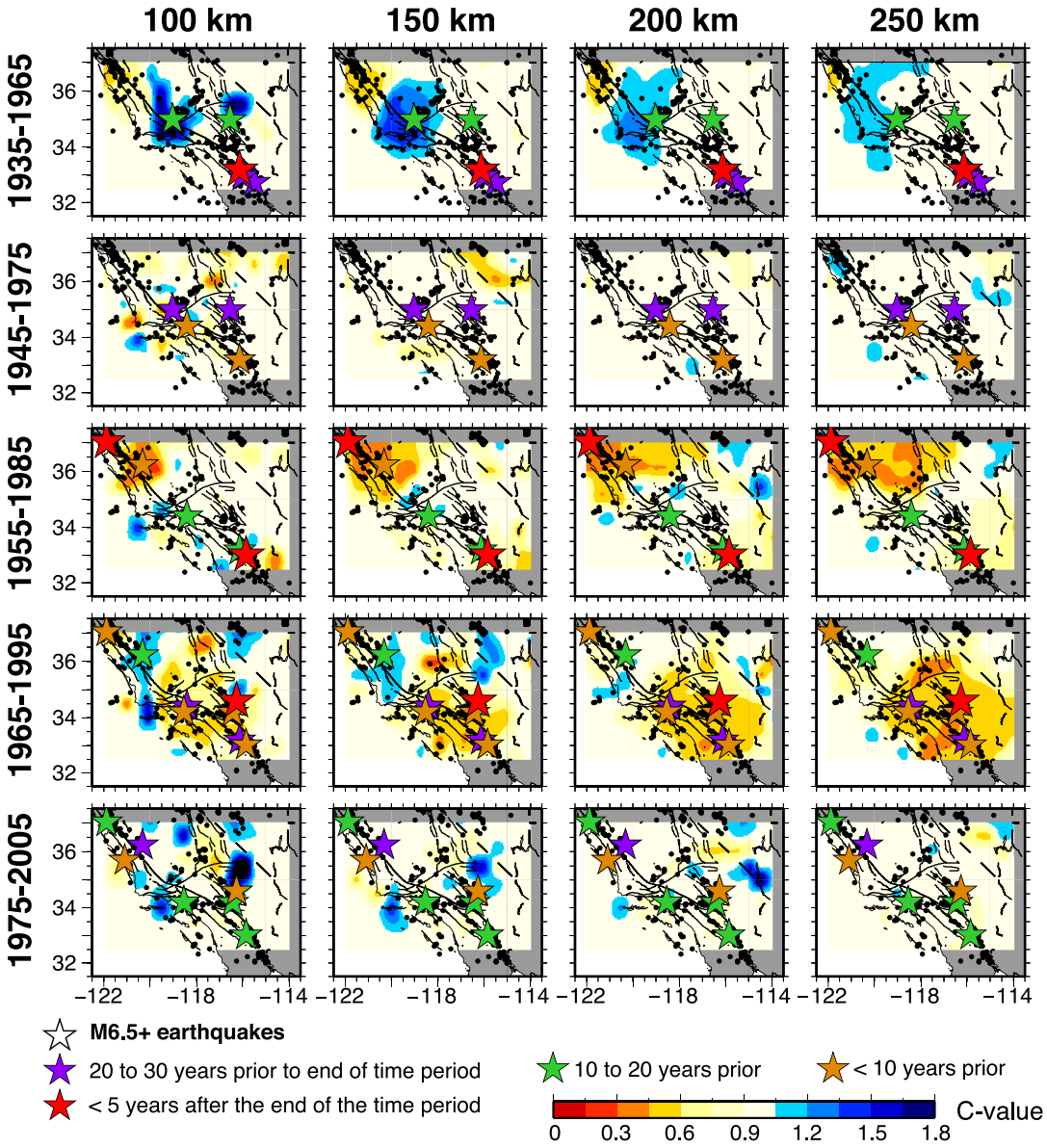

Figure 6. AMR grid search with fixed parameters between 1935 and 2005 in 30-yr intervals. Columns show search results for AMR based on seismicity within 100–250 km radius distances from potential epicentres located every 0.5° in latitude and longitude and at the end of the 30 yr considered as labelled on left from top to bottom. Black dots show the M4.5+ earthquakes considered in the calculation, stars represent M6.5+ earthquakes that occurred during the time period considered as well as within the next 5 yr, colour-coded with respect to the end of the time period scanned.

large (i.e. above 1.0) are relatively stable, independent of the search radius.

On the other hand, Fig. 6 shows very different patterns of the distribution of areas of high and low c-values when considering different time periods. This strong time dependence is the result of earthquake activity occurring in a given search region during the analysis period, in particular the large M6.5 events shown by purple, green and orange stars in Fig. 6. The occurrence of large earthquakes during the search period tends to influence the c-value depending on if they occur early (i.e. purple and green stars in Fig. 6) or late (i.e. orange stars in Fig. 6) in a given 30-yr period. Not surprisingly, we find that when one or several large earthquakes followed by their aftershock sequences occur early in the time period considered, the resulting cumulative Benioff strain will not be well fit with an accelerating power-law curve and the c-value will be high (see Fig. 4c). On the other hand, we observe the opposite pattern when major earthquakes occur near the end of the studied time range (Fig. 4a). In this case, the c-value will be low because of the increase in the slope of the cumulative Benioff strain towards the end of the analysis. For example, low c-values are found between 1965 and 1995 (Fig. 6) in a region south of 35°N latitude where three of five earthquakes with magnitude larger than 6.5 (i.e. the 1987 M6.7 Superstition Hills, 1992 M7.3 Landers and the 1994 M6.7 Northridge earthquakes) occurred after 1980, which corresponds to the middle of the analysed period. Of course, such large, late events could then be considered as the culmination of a stress accumulation cycle within their epicentral regions. This is also observed in Fig. 5(f) where the regions with the lowest c-values are found in the proximity of the 1989 Loma Prieta earthquake that occurred less than 3 yr before the 1992 Landers earthquake.

Finally, the latest period shown in Fig. 6 between 1975 and 2005 shows no significant areas of low *c*-values. Nonetheless, the *M*7.2 El Mayor–Cucapah earthquake struck northern Mexico (32.26°N–115.29°E) in 2010 April, just south of the area studied here in the grid search (white star in Fig. 1). The absence of low *c*-value in this region can be partly due to the occurrence of several *M*6.5+ in southern California, in the 1990s (green stars in Fig. 6).

4 AMR AND REGIONS OF STRESS INCREASES

4.1 AMR maps versus stress maps

According to the elastic rebound theory (Reid 1910), which states that stress accumulates over time along locked segments of faults and is suddenly released in an earthquake, it is important to understand the state of tectonic stress in seismically active regions as well as its temporal evolution. This motivated King & Bowman (2003) to propose an analysis explicitly focused on stress-accumulation patterns, by assuming complete stress drop on all fault segments surrounding a target rupture for which AMR is being examined. For this purpose, they calculate the stress fields associated with back-slip rupture models to better constrain the area of interest instead of using a simple circular search region. Because explicit connections are drawn between the evolution of stress and the AMR hypothesis, it would be appropriate to expect some degree of correlation between maps of modelled stress increases over the last two centuries and AMR behaviour over a region of interest prior to a major seismic event.

Fig. 7 presents maps of *c*-values from 1935 to 2005 (200 km radius from Fig. 6) directly compared to maps of the modelled stress state incorporating contributions of 200 yr of major historic earthquakes, post-seismic relaxation and interseismic strain (Freed *et al.* 2007). Areas inferred to be highly stressed (i.e. positive stress values shown in warm colour in Fig. 7), and thus presumably closer to a potential rupture that could be expected also show evidence of accelerating seismicity. As shown in Fig. 7(b), except for the contributions from the coseismic and post-seismic loading associated with the largest earthquakes (i.e. $M > 7$), there is only modest variation in the large-scale stress pattern with time over the relatively short time periods considered (i.e. 30-yr intervals). This contrasts with the *c*-value maps (Figs 6 and 7), which show strong time dependence.

4.2 AMR in highly stressed areas

To complete the analysis of AMR in southern California, we examine AMR in apparent high-stress regions ($\Delta\sigma$ >1 bars) in the models of Freed *et al.* (2007) between 1950 and 2010 (Fig. 8). We pose the hypothesis that regions that accumulated the largest Coulomb stress increases since 1812 represent the locations of potential events and where significant AMR should be observed if the AMR method were valid. Nonetheless, it is worth recalling that the state of stress in 1812 is unknown and that recurrence intervals on major faults in California are on the order of a few centuries. As we consider only seismicity since 1950, the tests are performed using events with magnitude larger than 3.5 for different time periods, each ending in 2009 December. It is possible here to lower the minimum magnitude from 4.5 to 3.5 to reflect the better coverage of the highly stressed areas located on the SAF system, which is relatively well monitored. We calculate the *c*-values in each case

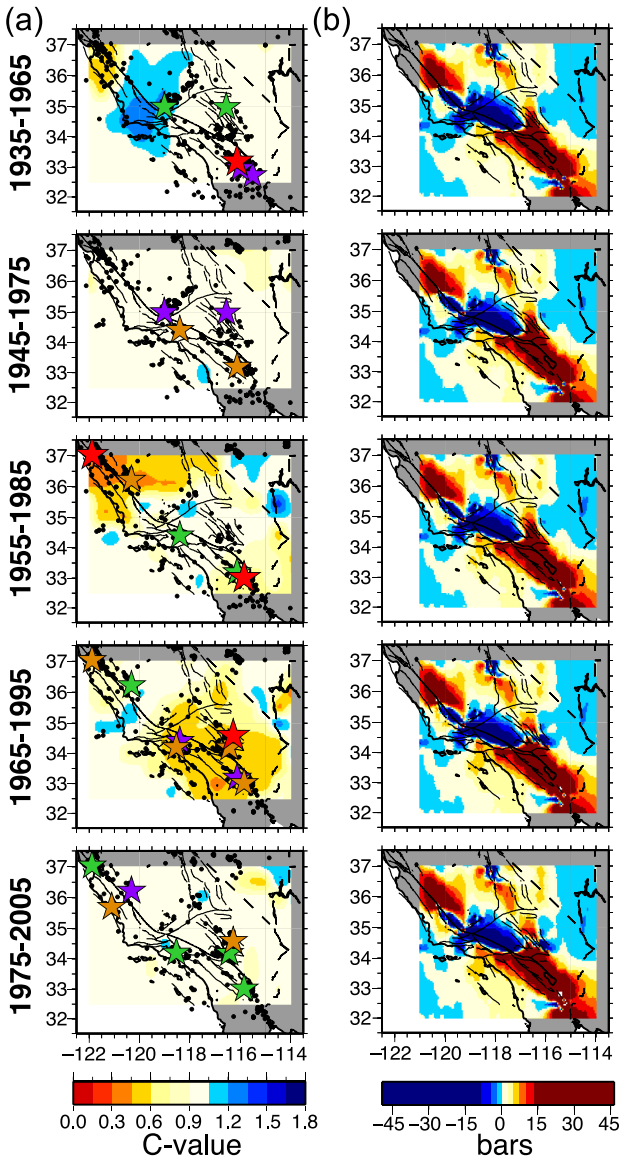

Figure 7. Comparison of the maps of the AMR grid search (a) and modelled stress changes (b) over time in southern California. (a) *c*-Values calculated for 200-km-radius regions for overlapping 30-yr periods as labelled on the left (see description Fig. 6). (b) State of Coulomb stress in bars in 1965, 1975, 1985, 1995 and 2005 (from top to bottom, respectively) at 8 km depth, computed considering coseismic stress transfers, post-seismic relaxation and interseismic loading in the crust and upper mantle, since 1812 (Freed *et al.* 2007).

considering a main shock in 2010 June (i.e. 6 months after the end of the analysed earthquake catalogue; Fig. 8).

The northern high-stress region, which corresponds to the larger Parkfield area that we study in more detail below, gives similar results as previously observed. Considering all events in zones of $\Delta\sigma > 1$ bar within the circled (150-km radius) area shown in Fig. 8(a), the *c*-values stay close to 1. The *c*-values decrease slightly (i.e. ∼0.7) for events at $\Delta\sigma \geq 30$ bars (Fig. 8b). It is worth recalling that this region of apparent high stress has to be considered carefully because it includes the southern section of the creeping SAF, which is not accounted for in the stress models. If we search for AMR in the southern highly stressed region (Fig. 8c) by considering the seismicity located where the change of stress is larger than 1 bar

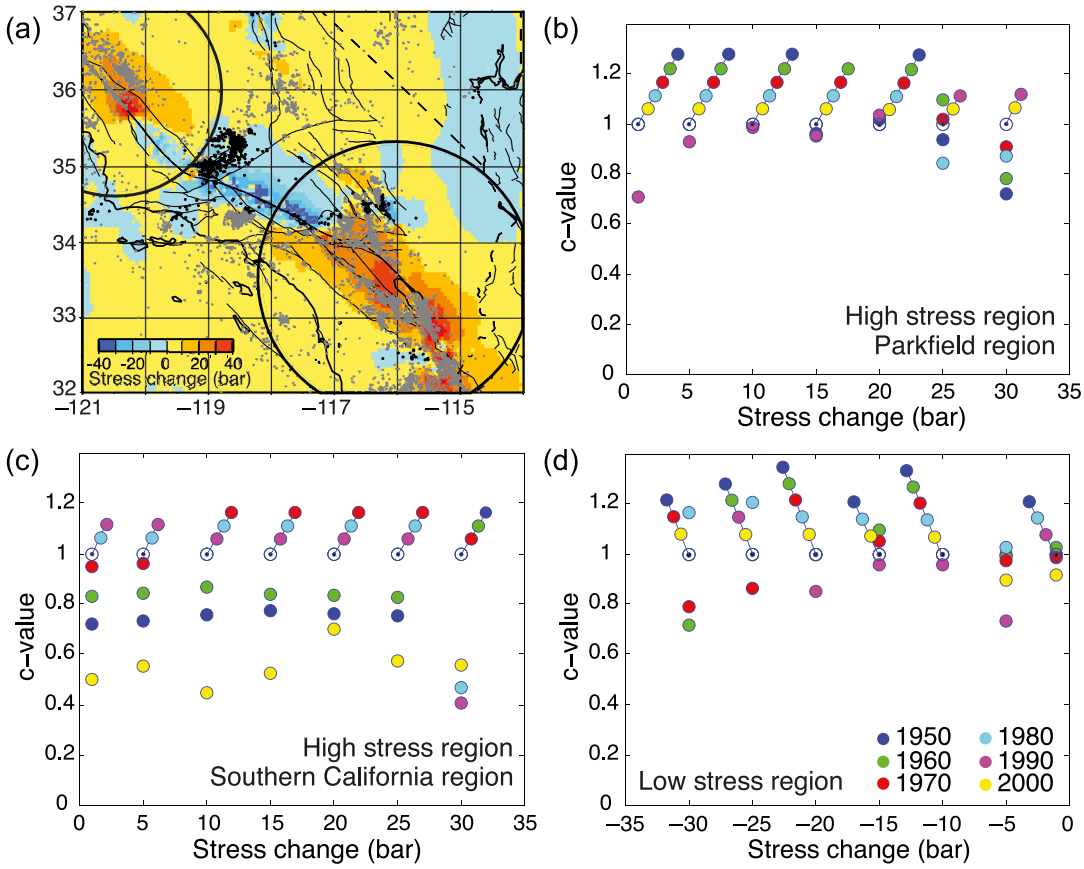

Figure 8. AMR in highly stressed regions. (a) Map of Coulomb stress changes on SAF-parallel strike-slip faults in southern California (Freed *et al.* 2007) computed for 2005. The $M > 3.5$ earthquakes from 1950 to 2009 located within regions with positive $\Delta\sigma$ are shown in grey, else in black. (b) c-Values obtained for events in zones of stress greater or equal to a range of values in the northern high-stress region with varying search-period starting times (end time: 2009 December). (c) c-Values obtained for the southern high-stress region. The circles in (a) indicate the extent of the zones considered in both apparent high-stress regions. (d) c-Values obtained for various time and stress conditions (start year for each variable-length search period is indicated by colour and c-values are computed for all events at stress less or equal to the value given).

within the 300-km radius area shown in Fig. 8(a), no clear case of AMR is observed (i.e. c-values between 0.7 and 1) except when considering events since 2000 and/or occurring at $\Delta\sigma \geq 30$ bars, for which c is found to be less than 0.6.

In summary, in the positively stressed regions of the mechanical model, the c-values are close to 1, independent of the time range and stress level. The only exception is found when earthquakes located in regions with 30+ bars stress changes are taken into account. Then, the c-values decrease slightly especially for the southernmost region of interest, along the SAF system, and for the more recent time ranges. The 2010 M7.2 El Mayor–Cucapah earthquake occurred within this high-stress region where the c-values have been below 0.6 since 1980. Its occurrence could be seen as consistent with the low c-values found in this high-stress region in the last 30 yr. However, we note that when using different search parameters, the c-value maps shown in Figs 6 and 7 do not indicate evidence for AMR in this southernmost region highlighting the sensitivity of the analysis to the parameters.

We also perform an AMR search in the areas of reduced stress ($\Delta\sigma \leq -1$ bars), due in large part to the enduring stress shadow of the great 1857 Fort Tejon earthquake (Fig. 8d). Once again, the detection of accelerating seismicity is variable depending on the time range considered. We find similar c-values like those previously obtained in the two high-stress regions (i.e. between 0.7 and 1). Because no difference is seen in evidence of AMR between the low and high-stress areas, these results suggest that current stress levels do not correlate with seismicity rate changes. The low-stress regions appear to show comparable evidence for AMR as the highly stressed regions. The lack of strong recent earthquakes in either the especially highly stressed/unstressed areas so far in our study region, with the possible exception of the M7.2 El Mayor–Cucapah earthquake, indicates that the obtained distribution of AMR does not appear to reflect regionally varying stress levels.

5 AMR ANALYSIS SPANNING THE 1967–2004 PARKFIELD EARTHQUAKE CYCLE

5.1 Circular analysis

Mignan *et al.* (2007) proposed a mathematical formulation of AMR using a stress accumulation model, which is based on the concept of the elastic rebound theory. AMR would result as the consequence of the decreasing size of the stress shadow generated by a previous earthquake. Such stress shadows following large seismic events have been revealed in several cases in California (Harris & Simpson 1996, 1998; Kenner & Segall 1999; Parsons 2002). Mignan *et al.* (2007) proposed that a steady acceleration of seismicity should be evident throughout the entire seismic cycle, but would become

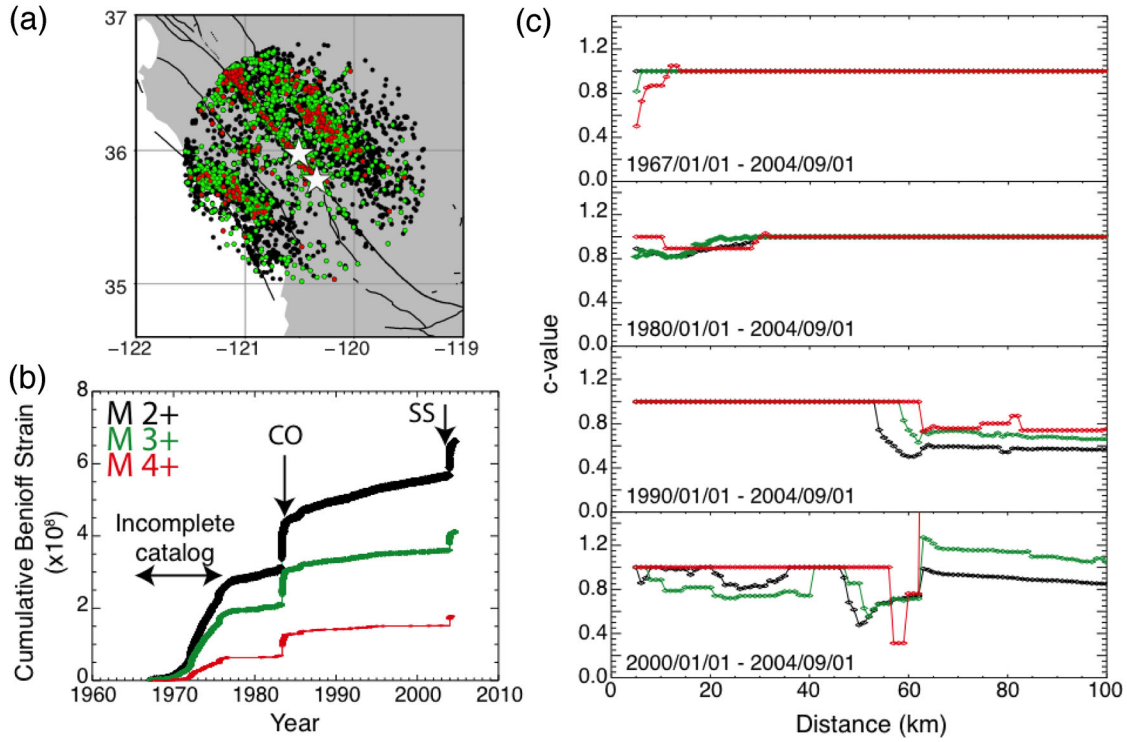

Figure 9. AMR analysis in the Parkfield region over the last *M*6 earthquake cycle on the SAF. (a) Map of the *M*2 (black), *M*3 (green) and *M*4 (red) earthquakes recorded between 1967 and 2004. The stars show the locations of the 1966 and 2004 Parkfield earthquakes. (b) Cumulative Benioff strain between 1967 and 2004 using different magnitude range earthquakes within 100-km distance from Parkfield. Network sensitivity changes in early 1970s and the occurrence of the 1983 Coalinga (CO) and 2003 San Simeon (SS) earthquakes explain large step increases in the cumulative Benioff strain. (c) Calculated *c*-values over the region between 1967 January and 2004 September using variable magnitude and distance ranges.

more pronounced later during the earthquake cycle. To demonstrate this is a difficult task, because of the long recurrence intervals for most fault segments in California and elsewhere—often on the order of several centuries for major earthquakes—and the lack of complete earthquake catalogues available for such studies. The Parkfield region in central California, which has been the site of several characteristic *M*6 earthquakes that have repeated over a relatively short earthquake cycle (∼24 yr on average) since 1857, represents a unique opportunity to evaluate changes in seismicity rate spanning full recurrence intervals (Wallace 1991; Bakun *et al.* 2005; Murray & Langbein 2006). Because the main shock is smaller in magnitude than the usual target events of prior AMR studies (i.e. $M \geq 6.5$), it requires lowering the minimum magnitude of the pre-events. Hardebeck *et al.* (2008) found that there is no systematic correlation between the main shock magnitude and the corresponding *c*-value. Moreover, dropping the target event magnitude to *M*6 should not affect the AMR behaviour because it should be magnitude invariant if based on a simple stress accumulation model.

We search for AMR during the last earthquake cycle between 1967 and 2004, using the ANSS seismicity catalogue with $M > 2.0$ in a 100-km radius region centred on the rupture zone of the *M*6 Parkfield earthquake. Computation of AMR in the area is performed using various magnitudes and distance ranges (Fig. 9). The completeness of the catalogue evolved with time over the region, especially in the early period of the cycle prior to 1975 (Fig. 9b). The magnitude of completeness over the 1967–2004 time period is ∼2.5, however when considering subsets of the catalogue we found that completeness is only obtained for *M*3 and larger between 1967 and 1980, but is reduced to ∼*M*2 between 1980 and 2004. Fig. 9(c) shows that no apparent acceleration of seismicity is observed between 1967 and 2004 independent of the cut-off magnitudes. The *c*-value is equal to 1 over most of the search radii (0–100 km; Fig. 9c).

According to Mignan *et al.* (2007), AMR might not be observable during an entire earthquake cycle either because of limited earthquake activity and/or because of its sensitivity to a few large earthquakes during a given time interval. We also search for AMR over shorter periods of time, which allow us to reach a minimum magnitude of 2 from 1980. We find that different time periods can significantly affect the *c*-value pattern (Fig. 9c). The AMR results are very sensitive to the occurrences of the nearby 1983 *M*6.5 Coalinga-Nunez and 2003 *M*6.5 San Simeon earthquakes and to their aftershock sequences. We find lower *c*-values after 1990 when the Coalinga-Nunez sequence is mostly removed from the analysis and when the San Simeon sequence dominates the earthquake activity in the latter part of the cycle at distances larger than 50 km. This illustrates the complex nature of the earthquake catalogue and the difficulties in trying to objectively estimate the seismicity evolution during this cycle. If AMR can be observed in the studied data set this again appears to strongly depend on choices made in the search parameters.

5.2 Analysis centred on the SAF

To properly test AMR in the Parkfield region, it may be important to focus more closely on the vicinity of the 1966 and 2004 ruptures, and on the area of expected stress accumulation on the rupture zone. Parkfield is located along a transitional section of the SAF with the main creeping segment of the fault from Parkfield to San Juan Bautista to the north and the fully locked portion of the fault

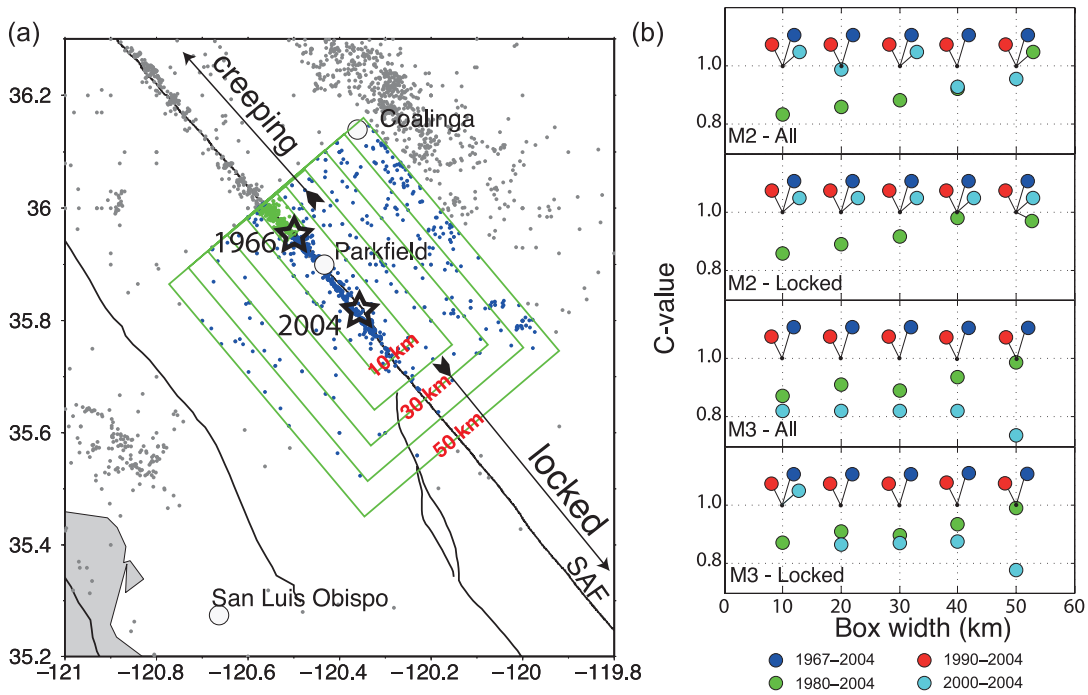

Figure 10. Variation of *c*-values in the restricted Parkfield rupture region. (a) Map of *M*2.0+ earthquakes between 1935 and 2010 (grey), located within the boxes centred on the SAF in the locked section (blue), and within a 5-km wide segment on the creeping segment from the 1966 Parkfield earthquake epicentre northwards (green). The smaller box has dimensions of 40 km by 10 km. Others are 10 km larger in both sides, up to 50 km wide. The stars locate the 1966 and 2004 Parkfield earthquakes. (b) Variation of *c*-value for the 1967–2004 earthquake cycle as a function of time and box size. All means blue and green earthquakes from (a). Locked means blue earthquakes only.

that last ruptured in the 1857 Fort Tejon earthquake to the south (Wallace 1991). The successive 1934, 1966 and 2004 Parkfield ruptures were collocated with similar dimensions as modelled by Murray & Langbein (2006) (see their fig. 5). We define an initial rectangular 40 km-by-10 km search area to encompass the historic Parkfield rupture areas (Murray & Langbein 2006; Kim & Dreger 2008) along the fault (Fig. 10). This area roughly delimits the region of stress accumulation in a simple mechanical model of free creep to the north and the locked Cholame Fault segment to the south. We evaluate the seismicity change within successive boxes incremented by 10 km on all sides centred on the segment, while fixing the boundary to the northwest where the SAF is fully creeping. We also evaluate the influence of the small creeping portion of the SAF included in the boxes (green seismicity in Fig. 10a) by comparing the *c*-values obtained when using all the encompassed seismicity and events located only in the locked region (blue earthquakes in Fig. 10a compared to the blue and green events). The 1966 Parkfield epicentre near Middle Mountain corresponds to the starting location of the creeping section to the north (Murray & Langbein 2006), and marks the southern extent of the 5-km wide box (Fig. 10a).

Fig. 10(b) shows that the *c*-values calculated for the rectangular search areas vary over different time and distance ranges using $M > 2$ and $M > 3$ earthquakes. Nonetheless, the *c*-values are close to 1 and indicate no evident acceleration of seismicity. The lowest *c*-values are found between 1980 and 2004, using $M > 2$ and $M > 3$ earthquakes, and between 2000 and 2004 for the $M > 3$ earthquakes only. However, they progressively approach 1 between 1980 and 2004 with extending box width as the selected region approached the rupture zone of the 1983 Coalinga earthquakes (Fig. 9). In addition, when using earthquakes since 2000, lower *c*-values are observed without passing beneath the 0.7 threshold value for AMR detection. Based on the results of the analysis no conclusive acceleration of seismicity is observed using both small and larger areas in this short earthquake cycle region.

6 DISCUSSION AND CONCLUSIONS

The findings of AMR are strongly dependent on the choices of the three parameters used (i.e. magnitude, time interval and search area ranges) to calculate the cumulative Benioff strain relative to target events of interest. We find that once the parameters have been found to best support an acceleration of seismicity before three historic earthquakes, they are specific to these events and do not suggest AMR elsewhere in the region except in the target event locations (Fig. 5). This is somewhat encouraging because it suggests the specificity of the solution to the location of the target main shock instead of diverging to other regions and potentially resulting in false alarms. However, because the parameters are specific to a chosen main shock, it becomes difficult to use this AMR approach in a more general way. When fixing the parameters for the three large earthquakes in question to common values, the results differ significantly and indicate no AMR prior to these events. Moreover, to use AMR in a direct manner for earthquake forecasting, independent parameters are required without an *a priori* knowledge of the expected earthquake magnitude and location. An attempt to search for AMR under such conditions was performed over the entire region of southern California between 1950 and 2005. Even though we tested a range of common search radii, we find that out of the main shocks occurring within 5 yr after the end of the tested periods, only the 1989 Loma Prieta was located in a wide low *c*-value area (Fig. 5). Such results show the limitation of the method in term of practical earthquake forecasting. Finding systematic relationships between the search variables and the magnitude of the target events

would be the key for successful AMR detection. Without these, this hypothesis remains no more than a data-fitting exercise that has to be retrospectively tailored to each event (Hardebeck *et al.* 2008).

As previously noted by Hardebeck *et al.* (2008), we demonstrate that the outcome of AMR analyses (i.e. *c*-value determination) is dominated by the occurrence of a few large earthquakes during the studied period (i.e. 30-yr long, Fig. 5). Indeed, a large event at the beginning of a chosen observation cycle tends to dominate the cumulative Benioff strain and will result in an increase of the *c*-value (Fig. 5). On the other hand, a main shock and its following aftershock sequence occurring near the end of the time period tend to significantly decrease the *c*-value and support the case for AMR. We find that calculated values for AMR vary dramatically with time due to *c*-values being strongly influenced by the small number of moderate to large events in the historic record.

This leads to the question of whether or not to decluster the earthquake catalogue. This remains a controversial option as AMR has been observed in previous studies on both complete and declustered catalogues (Mignan 2011, and references therein). Declustering might appear as a solution to obtain an image of the evolution of seismicity that is less biased by large events and their aftershocks (Matthews & Reasenberg 1988). Nonetheless main shocks and aftershock sequences are important components of the seismic activity and evolving moment release of a region. They can generate stress changes that can act as potential triggers of large earthquakes. The 1992 *M*7.3 Landers earthquake for example was preceded by the *M*6.1 Joshua Tree earthquake, which struck the region 2 months earlier, and was followed 3 hr later by the *M*6.3 Big Bear earthquake (Hauksson *et al.* 1993). In this study, we chose to not decluster the earthquake catalogue. Even if the catalogue can be more or less modified to account for seismic clusters, it appears that the choice of declustering the catalogue or not would correspond to another parameter that would need to be considered in the analysis. Because opposite results may be observed before and after declustering, this would represent another free parameter in a 'data-fitting' analysis.

AMR appeared to be an appropriate methodology for earthquake forecasting, because it is based on the stress evolution on a fault (Bowman *et al.* 1998; Bowman & King 2001; King & Bowman 2003). Each earthquake releases stress over some volume in its surrounding neighbourhood and AMR has been explicitly linked to static stress build-up and release in this volume (e.g. Bowman & King 2001; Mignan *et al.* 2006a). For a very simple system of an isolated rupture asperity under increasing load, it makes sense to expect AMR, or accelerating seismic activity in general, in areas of rising stress through the earthquake cycle (King & Bowman 2003; Mignan 2011). A possible example of such an idealized simple system may be the sequence of repeating $M \approx 4.9$ earthquakes in northeast Japan that are embedded in an otherwise aseismically slipping portion of the subduction thrust (Uchida *et al.* 2007). There, each of the five recurrences of the main shock rupture was preceded by accelerating levels of microseismicity in the immediate vicinity of the rupture (Uchida *et al.* 2007, 2012). On the other hand, we are unsuccessful in determining such acceleration in the earthquake occurrences prior to the 2004 Parkfield earthquake, even when we focus the analysis on the SAF and its immediate surroundings to decrease the effects of regional large events (Fig. 10). Independent of the time period considered (i.e. from less than 4 yr to the full recurrence interval of 37 yr) and of the size of the search region, the observed *c*-values remain close to 1. Moreover, when we explicitly evaluate AMR in areas of high stress indicated by a stress evolution model that takes into consideration 200 yr of stress change from coseismic, post-seismic and interseismic loading in southern California, no correlations are found between the AMR results and the modelled stress levels in the region. Even if the studied stress changes are not an accurate representation of the total stress, because of the lack of knowledge of the state of stress prior to 1812 and because of various model assumptions used for the stress calculations, the areas that sustained stress increases that approach plausible stress drop values should be closer to failure and should differ from *c*-values obtained from a random earthquake catalogue analysis (i.e. close to 1). This indicates that the more complex geometry and mechanics of most active fault systems in the world may simply not lend themselves to producing such simple patterns of stress and seismicity evolution as considered in the description of AMR (King & Bowman 2003). A better understanding of the physical process is still needed (Mignan 2011, 2012).

Because of the numerous inconclusive results from past AMR studies, the AMR hypothesis has been widely criticized (Michael *et al.* 2006; Hardebeck *et al.* 2008; Hough 2009). Nonetheless, AMR has been reported in physically motivated models, which demonstrated that a power-law relationship for Benioff strain prior to large ruptures can be observed in model systems when the seismicity has broad frequency-size statistics (Ben-Zion & Lyakhovsky 2002). New approaches have been suggested for the study of seismic activity changes prior to large earthquakes (Mignan & Di Giovambattista 2008; Mignan 2011, 2012). Instead of focusing only on the acceleration of seismicity through the earthquake cycle, these studies try to integrate a number of potential precursory phenomena such as seismic quiescence (Wyss & Habermann 1988), seismicity acceleration and the spatial organization of precursory seismicity around a pending rupture zone (i.e. the 'Mogi doughnut') (Kanamori 1981). Using synthetic catalogues and a couple of earthquakes in Italy including the 2009 *M*6.3 L'Aquilla earthquake, they showed that the acceleration of seismicity and precursory quiescence occur in the same space–time window. The acceleration can thus be observed when fixing the region of interest to the region in which the quiescence is observed, and the time period since the beginning of the quiescence (i.e. less than 2 yr prior to the L'Aquilla earthquake). This is an interesting result as it shows a short-term activation of the seismicity, and tries to objectively define two of the parameters that highly affect the AMR results. This contrasts from the long-term activation previously published (Bowman *et al.* 1998). Wyss *et al.* (1990) identified a period of seismic quiescence at Parkfield and announced that based on other cases of precursory quiescence, the *M*6 Parkfield earthquake should be expected in the 2 yr following their publication. However, the Parkfield earthquake occurred 14 yr later. Analysis of AMR in this same time period does not reveal such seismic increase (Figs 9 and 10). More analyses should be conducted to properly test the hypothesis proposed by Mignan (2012). In particular, the identification of seismic quiescence before large earthquakes is critical in this method, especially in a routine, forecasting approach.

To conclude, the lack of systematic relationships between the search parameters used in determining AMR and the size of a main shock, the observation of both accelerating and decelerating seismicity for the same target events depending on changes in these parameters, and the absence of clear distinction of the AMR pattern in areas of high and low stress determined independently from mechanical models of southern California suggest that the evaluation of AMR as is has little practical value for earthquake forecasting purposes. Our grid-based analysis using a range of fixed search parameters indicates little promise for using this AMR approach in earthquake forecasting. The spatiotemporal juxtaposition of different earthquake recurrence times and fault zones is not consistent

with the idealized model proposed by Bowman *et al.* (1998) and Bowman & King (2001), which considers stress on a simple single fault plane. Even when considering a relatively detailed model of stress accumulation due to interseismic, coseismic and post-seismic deformation spanning two centuries, we fail to find convincing correlation of changes in the seismicity rate with areas of high stress. Thus, even if seismicity rates do reflect the magnitude of ambient stress, they may be of limited value for practical earthquake hazard analysis in southern California where different scale fault systems interact in an as-of-yet unpredictable fashion. Better understanding of earthquake source physics and interaction, as well as longer earthquake catalogues with low magnitudes of completeness might provide valuable information on precursory seismicity pattern, and help in finding this Holy Grail of earthquake forecasting research.

ACKNOWLEDGEMENTS

This research was supported by the Southern California Earthquake Center (SCEC). SCEC is funded by NSF Cooperative Agreement EAR-0529922 and USGS Cooperative Agreement 07HQAG0008. The SCEC contribution number for this paper is 1695. We thank Arnaud Mignan, GJI editor Ingo Grevemeyer and two anonymous reviewers for their constructive comments. Berkeley Seismological Laboratory contribution number 13-01.

REFERENCES

Bakun, W.H. *et al.*, 2005. Implications for prediction and hazard assessment from the 2004 Parkfield earthquake, *Nature,* **437,** 969–974.

Ben-Zion, Y. & Lyakhovsky, V., 2002. Accelerated seismic release and related aspects of seismicity patterns on earthquake faults, *Pure appl.Geophys.,* **159**(10), 2385–2412.

Bouchon, M., Durand, V., Marsan, D., Karabulut, H. & Schmittbuhl, J., 2013. The long precursory phase of most large interpolate earthquakes, *Nature Geosci.,* **6,** 299–302.

Bowman, D.D. & King, G.C.P., 2001. Accelerating seismicity and stress accumulation before large earthquakes, *Geophys. Res. Lett.,* **28,** 4039–4042.

Bowman, D.D., Ouillon, G., Sammis, C.G., Sornette, A. & Sornette, D., 1998. An observational test of the critical earthquake concept, *J. geophys. Res.,* **103**(B10), 24 349–24 372.

Bufe, C.G. & Varnes, D.J., 1993. Predictive modeling of the seismic cycle of the greater San Francisco Bay region, *J. geophys. Res.,* **98,** 9871–9883.

Deng, J. & Sykes, L.R., 1997. Evolution of the stress field in southern California and triggering of moderate-size earthquakes: a 200-year perspective, *J. geophys. Res.,* **102,** 9859–9886.

De Santis, A., Cianchini, G., Qamili, E. & Frepoli, A., 2010. The 2009 L'Aquila (central Italy) seismic sequence as a chaotic process, *Tectonophysics,* **496,** doi:10.1016/j.tecto.2010.10.005.

Ellsworth, W.L., Lindh, A.G., Prescott, W.H. & Herd, D.G., 1981. The 1906 San Francisco earthquake and the earthquake cycle, in *Earthquake Prediction,* eds Simpson, D.W. & Richards, P.G., American Geophysical Union.

Freed, A.M., Ali, S.T. & Burgmann, R., 2007. Evolution of stress in Southern California for the past 200 years from coseismic, postseismic and interseismic stress changes, *Geophys. J. Int.,* **169,** doi:10.1111/j.1365-1246X.2007.03391.x.

Hardebeck, J.L., Felzer, K.R. & Michael, A.J., 2008. Improved tests reveal that the accelerating moment release hypothesis is statistically insignificant, *J. geophys. Res.,* **113,** B08310, doi:10.1029/2007JB005410.

Harris, R.A. & Simpson, R.W., 1996. In the shadow of 1857: the effect of the great Ft.Tejon earthquake on subsequent earthquakes in southern California, *Geophys. Res. Lett.,* **23,** 229–232.

Harris, R.A. & Simpson, R.W., 1998. Suppression of large earthquakes by stress shadows: a comparison of Coulomb and rate-and-state failure, *J. geophys. Res.,* **103,** 24 439–24 451.

Hauksson, E., Jones, L.M., Hutton, K. & Ederhart-Phillips, D., 1993. The 1992 Landers earthquake sequence: seismological observation, *J. geophys. Res.,* **98**(B11), 19 835–19 858.

Hough, S., 2009. *Predicting the Unpredictable: The Tumultuous Science of Earthquake Prediction,* Princeton University Press.

Jiang, C. & Wu, Z., 2005. Test of the preshock accelerating moment release (AMR) in the case of the 26 December 2004 Mw9.0 Indonesia Earthquake, *Bull. seism. Soc. Am.,* **95**(5), 2016–2025.

Jiang, C. & Wu, Z., 2006. Benioff strain release before earthquakes in China: accelerating of not? *Pure appl. Geophys.,* **163,** 1965–1976.

Kanamori, H., 1981. The nature of seismicity patterns before large earthquakes, in *Earthquake Prediction: An International Review,* pp. 1–19, eds Simpson, D.W. & Richards, P.G., American Geophysical Review.

Kanamori, H. & Anderson, D.L., 1975. Theoretical basis of some empirical relations in Seismology, *Bull. seism. Soc. Am.,* **65**(5), 1073–1095.

Kenner, S. & Segall, P., 1999. Time-dependence of the stress shadowing effect and its relation to the structure of the lower crust, *Geology,* **27**(2), 119–122.

Kim, A. & Dreger, D.S., 2008. Rupture process of the 2004 Parkfield earthquake from near-fault seismic waveform and geodetic records, *J. Geophys. Res.,* **113,** B07308, doi:10.1029/2007JB005115.

King, G.C.P. & Bowman, D., 2003. The evolution of regional seismicity between large earthquakes, *J. geophys. Res.,* **108,** doi:10.1029/2001JB000783.

Lindh, A.G., 1990. The seismic cycle pursued, *Nature,* **348,** 580–581.

Matthews, M.V. & Reasenberg, P.A., 1988. Statistical methods for investigating quiescence and other temporal seismicity patterns, *Pure appl. Geophys.,* **126**(2–4), 357–372.

Michael, A.J., Hardebeck, J.L. & Felzer, K.R., 2006. Precursory accelerating moment release: an artifact of data-selection, *EOS, Trans. Am. geophys. Un.,* **87**(52), Fall Meet. Suppl., Abstract S24A-02.

Mignan, A., 2008. Non-Critical Precursory Accelerating Seismicity Theory (NC PAST) and limits of the power-law fit methodology, *Tectonophysics,* **452,** 42–50.

Mignan, A., 2011. Retrospective on the Accelerating Seismic Release (ASR) hypothesis: controversy and new horizons, *Tectonophysics,* **505,** 1–16.

Mignan, A., 2012. Seismicity precursors to large earthquakes unified in a stress accumulation framework, *Geophys. Res. Lett.,* **39,** L21308, doi:10.1029/2012GL053946.

Mignan, A. & Di Giovambattista, R., 2008. Relationship between accelerating seismicity and quiescence, two precursors to large earthquakes, *Geophys. Res. Lett.,* **35,** L15306, doi:10.1029/2008GL035024.

Mignan, A., Bowman, D.D. & King, G.C.P., 2006a. An observational test of the origin of accelerating moment release before large earthquakes, *J. geophys. Res.,* **111,** B11304, doi:10.1029/2006JB004374.

Mignan, A., King, G., Bowman, D., Lacassin, R. & Dmowska, R., 2006b. Seismic activity in the Sumatra-Java region prior to the December 26, 2004 (M_w = 9.0–9.3) and March 28, 2005 (M_w = 8.7) earthquakes, *Earth planet. Sci. Lett.,* **244,** 639–654.

Mignan, A., King, G.C.P. & Bowman, D., 2007. A mathematical formulation of accelerating moment release based on the stress accumulation model, *J. geophys. Res.,* **112,** B07308, doi:10.1029/2006JB004671.

Murray, J. & Langbein, J., 2006. Slip on the San Andreas Fault at Parkfield, California, over two earthquake cycles, and the implications for seismic hazards, *Bull. seism. Soc. Am.,* **96**(4B), S283–S303.

Nutcracker v.X.1.5, Available at: http://earthscience.fullerton.edu/dbowman/Site/Downloads.html (last accessed 6 August 2013).

Parsons, T., 2002. Post-1906 stress recovery of the San Andreas fault system calculated from three-dimensional finite element analysis, *J. geophys. Res.,* **107**(B8), 2162, doi:10.1029/2001JB001051.

Pollitz, F.F. & Sacks, I.S., 1995. Consequences of stress changes following the 1891 Nobi earthquake, Japan, *Bull. seism. Soc. Am.,* **85**(3), 796–807.

Reid, H.F., 1910. *The Mechanics of the Earthquake,* in The California Earthquake of April 18, 1906: Report of the State Earthquake Investigation

Commission. Carnegie Institution of Washington Publication 87, 192 p. (reprinted in 1969).

Ryder, I. & Bürgmann, R., 2008. Spatial variations in slip deficit on the central San Andreas Fault from InSAR, *Geophys. J. Int.,* **175**(3), 837–852.

Sammis, C.G., Bowman, D. & King, G.C.P., 2004. Anomalous seismicity and accelerating moment release preceding the 2001 and 2002 earthquakes in Northern Baja California, Mexico, *Pure appl. geophys.,* **161,** 2369–2378.

Sykes, L.R. & Jaumé, S., 1990. Seismic activity on neighboring faults as a long-term precursor to large earthquakes in the San Francisco Bay Area, *Nature,* **348,** 595–599.

Toppozada, T.R. & Branum, D.M., 2002. California earthquakes of M ≥ 5.5: their history and the areas damaged, in *International Handbook of Earthquake and Engineering Seismology, part A,* pp. 793–796, eds Lee, W.H.K., Kanamori, H., Jennings, P.C. & Kisslinger, C., Academic Press.

Uchida, N., Matsuzawa, T., Ellsworth, W.L., Imanishi, K., Okada, T. & Hasegawa, A., 2007. Source parameters of a M4.8 and its accompanying repeating earthquakes off Kamaishi, NE Japan—implications for the hierarchical structure of asperities and earthquake cycle, *Geophys. Res. Lett.,* **34,** doi:10.1029/2007GL031263.

Uchida, N., Matsuzawa, T., Ellsworth, W.L., Imanishi, K., Shimamura, K. & Hasegawa, A., 2012. Source parameters of microearthquakes on an intraplate asperity off Kamaishi, NE Japan over two earthquake cycles, *Geophys. J. Int.,* **189**(2), 999–1014.

Wallace, R.E., 1991. The San Andreas Fault System, U.S. Geological Survey professional paper: 1515, edited by United States Government Printing Office, Washington, 1990.

Wang, Y., Yin, C., Mora, P., Yin, X.-C. & Peng, K., 2004. Spatio-temporal scanning and statistical test of the accelerating moment release (AMR) model using Australian Earthquake Data, *Pure appl. Geophys.,* **161,** 2281–2293.

Wyss, M. & Habermann, R.E., 1988. Precursory seismic quiescence, *Pure appl. Geophys.,* **126,** 319–332.

Wyss, M., Bodin, P. & Habermann, R.E., 1990. Seismic quiescence at Parkfield: an independent indication of imminent earthquake, *Nature,* **345,** 426–428.